Energy & Environmental Science

RSC Publishing

COMMUNICATION

View Article Online
View Journal | View Issue

Size-related native defect engineering in high intensity ultrasonication of nanoparticles for photoelectrochemical water splitting†

Cite this: *Energy Environ. Sci.*, 2013, **6**, 799

Received 12th November 2012
Accepted 10th January 2013

DOI: 10.1039/c3ee24058d

www.rsc.org/ees

Hongqiang Wang,*[a] Lichao Jia,[cd] Peter Bogdanoff,[c] Sebastian Fiechter,[c] Helmuth Möhwald[a] and Dmitry Shchukin[ab]

We report for the first time the demonstration of high intensity sonication treatment as a simple and effective way to fundamentally improve the performance of nanoparticles for photoelectrochemical (PEC) water splitting. The capability of making highly photoactive nanoparticles by high intensity sonication is highly appreciated to open up new opportunities in various areas, including PEC water splitting, dye-sensitized solar cells, and photocatalysis.

Broader context

Manipulation of electronic structures in nanostructured semiconductors is a key issue for improving their performance in optics, magnetics, electronics, and optoelectronics. We present in this paper that microscopically localized annealing by high intensity acoustic cavitation makes possible an interesting size-related native defect engineering in ZnO nanoparticles, which have been further adopted in photoelectrochemical (PEC) water splitting and achieved successfully tunable PEC performance. Since the critical particle size for nuclei of cavitation bubble is hundreds of nanometers, particle size dependent cavity nucleation is proposed for understanding the observed size-related variation of native defects. Furthermore, the tunable PEC performance can be explained by the sonication induced fluctuation of shallow/deep energy level defect concentrations, which can be applied for designing future high performance PEC devices. We believe that the sonication induced native defect engineering presented in this study will provide a new alternative for improving semiconductor electronic structures and will advance the study of nanoparticle based PEC water splitting.

Over the past few decades, considerable endeavors have been devoted to the solar-harvesting devices that may become an important source of sustainable energy.[1] Application of metal oxides such as photoanodes in photoelectrochemical cells (PEC) for water splitting has been one of the intensively investigated subjects.[2] Diverse efforts have been made to engineer nanostructured photoanodes with desired dimensions (*e.g.* nanowires, nanotubes), porosity or hierarchical structures, aiming to increase the effective surface area and to reduce carrier diffusion lengths.[3] On the other hand, improving the electronic structure of metal oxides is considered more important than improving morphological factors for effective production, separation, transportation and collection of photoexcited charge carriers.[4] Elemental doping is one versatile approach to modify the electronic structure of large band gap metal oxides for improving the optical extinction coefficient or enhancing the electrical conductivity.[5] However, doping wide-band gap oxides to enhance the visible-light response/electrical conductivity does not always result in higher overall efficiencies due to the high density of trap states for electron–hole recombination when optically active deep donors or acceptors are introduced.[6] Since native defects have a similar influence on the optical, electrical and catalytic properties as dopants, research interests have recently been shifted to manipulation of native defects by thermal treatment to enhance PEC cell performance.[7] Exploring strategies for native defect engineering under mild conditions such as low temperature and understanding the relationship between native defects and PEC cell performance are thereby challenging issues for designing high performance PEC devices.

High intensity ultrasonication has been of particular interest for the development of new materials and fabrication of novel nanostructures.[8] Both the physical and chemical effects of ultrasound arise from acoustic cavitation: the formation, growth, and collapse of bubbles in liquids irradiated with high intensity ultrasound.[9] One of the interesting subjects is the interaction between acoustic cavitation and solid targets because cavitation at liquid–solid interfaces is quite different

[a]*Max Planck Institute of Colloids and Interfaces, 14424 Potsdam, Germany. E-mail: Hongqiang.Wang@mpikg.mpg.de; Fax: +49 331 567-9202*

[b]*Stephenson Institute for Renewable Energy, Department of Chemistry, University of Liverpool, Crown Street, Liverpool, L69 7ZD, UK*

[c]*Helmholtz-Zentrum Berlin für Materialien and Energie, Institute Solar Fuels, Hahn-Meitner-Platz 1, 14109 Berlin, Germany*

[d]*Key Laboratory of Materials Physics, Anhui Key Laboratory of Nanomaterials and Nanotechnology, Institute of Solid State Physics, Chinese Academy of Sciences, Hefei, 230031, P. R. China*

† Electronic supplementary information (ESI) available: SEM, XRD, DLS, and PL analysis of ZnO nanoparticles before and after sonication. See DOI: 10.1039/c3ee24058d

from that in pure liquids,[8c] in which the effects of sonication demonstrate large variation depending on the size of the solid targets. For example, if liquids containing solids with extended surface area irradiated with ultrasound, cavity collapse becomes nonspherical at the liquid–solid interface driving high-speed jets of liquid onto the solid surface, and this has been utilized for the fabrication of porous surfaces;[10] if the target solids are micrometer sized, high-velocity interparticle collisions occur during ultrasonic irradiation of liquid–powder suspensions;[11] for micrometer sized soft matter, such as polyelectrolyte microcapsules, high intensity ultrasonic treatment can easily destroy the shells of polyelectrolyte microcapsules and thereby provide the release of the encapsulated material;[12] if the target solid approaches nanometer size, interparticle collision/fusion can only occur with the assistance of surfactants, which makes the particle surface hydrophobic for better accumulation at the gas/water cavitation boundary.[13] Despite intensive studies devoted to the sonication of solid targets, however, little research has been directed to sonication induced electronic structural evolution of bare nanoparticles,[14] which is of fundamental interest and practical importance for designing and constructing nanoparticle based nanodevices.

Herein, we present an innovative localized instantaneous annealing involved in high intensity sonication of nanoparticles, which is found encouragingly useful for improving semiconductor electronic structures for PEC applications. As far as we know, this is the first demonstration of native defect engineering achieved at room temperature leading to tuneable PEC performance, and it can thus be applied for designing future high performance PEC devices. Since manipulation of electronic structures in nanostructured semiconductors is a general key issue for improving their performance in optics, magnetics, electronics, and optoelectronics, high intensity sonication is highly appreciated as an attractive alternative to advance the electronic structure engineering in semiconductors for extensive applications.

We choose ZnO nanoparticles with three different sizes as sonication targets, given by the manufacturer: <50 nm, 100 nm, and <5 μm, which is named here as Sample 1 (S1), Sample 2 (S2), and Sample 3 (S3), respectively. Each kind of raw nanoparticles was first subjected to high intensity sonication with three different intensities (63 W cm^{-2}, 86 W cm^{-2}, 113 W cm^{-2}). As seen from Fig. S1 (ESI†), after sonication with different intensities, no morphological variation was observed for all three raw nanoparticles. Ultrasonically treated ZnO nanoparticles were further studied by X-ray diffraction (XRD, Fig. S2, ESI†) to gain insight into the size and phase evolution, and it was found that before and after sonication all nanoparticles have the wurtzite (hexagonal) ZnO structure, indicating that sonication has no influence on the phase evolution of ZnO nanoparticles. As the correlation length determined from the FWHM (full width at half maximum) corresponds to the crystal size, crystal sizes were thus calculated from the strongest diffraction peak (101) on the basis of the Debye Scherrer equation (Table T1, ESI†). The calculated average crystal sizes were 34 nm, 49 nm, and 105 nm for S1, S2 and S3, respectively, and crystal sizes showed not much difference for all of sonication treated samples when compared to that of original particles, revealing that the sonication treatment has nearly no influence on size change of the ZnO nanoparticles.

Fig. 1 shows UV-Vis spectra of the three kinds of ZnO nanoparticles before and after sonication with different intensities. It can be clearly seen from Fig. 1a that the optical extinction peak of S1 (367 nm) was not changed upon sonication. The intensity independent decrease of the extinction tail at high wavelengths that originates from Rayleigh scattering indicates that sonication reduces aggregation, and this effect is sonication-intensity independent. As seen in Fig. 1b, the extinction peaks are always at 375 nm for S2 with and without sonication treatment. After a careful examination, it can be observed that sonication induced fragmentation for S2 is slightly intensity-dependent, as the intensities of the extinction tails slightly decrease with increasing intensity. A different optical extinction behavior was found for S3, as seen in Fig. 1c. The tails of the extinction curves at the long wavelength range are not hyperbolic (typical for Rayleigh Scattering) any more but rather linear. This is understood if one considers that the average size of S3 is nearly comparable with the visible light

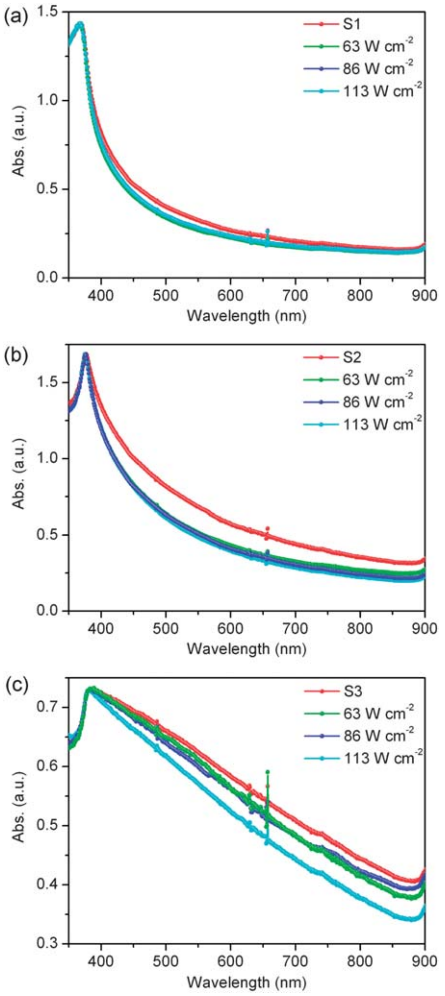

Fig. 1 UV-Vis spectra of differently sized ZnO particles (a) S1, (b) S2, and (c) S3 before and after high intensity ultrasonication with different intensities (63, 86, and 113 W cm^{-2}).

wavelength, the scattering curves are thus at the boundary of Rayleigh Scattering and Mie Scattering. It can also be observed that sonication treated S3 with different intensities has the same extinction peak, which is located at 381 nm. The extinction peaks in Fig. 1a–c show a red-shift, which is crystal size related and in agreement with the previous report.[15] The sonication induced fragmentation for S3 is obviously intensity dependent, as the intensities of extinction tails gradually decrease with increasing sonication intensities.

The above results can be proved by the results of dynamic light scattering (DLS), which was used to investigate the average sizes of ZnO nanoparticles dispersed in liquid before and after sonication. As seen from Table T2 (ESI†), all three untreated nanoparticles are aggregated judging from the large average sizes obtained from DLS. After sonication, average sizes of all nanoparticles decrease due to fragmentation by ultrasound. Different from S1, S2 and S3 reveal sonication-intensity dependent fragmentation, which agrees well with the UV-Vis results.

Based on the above analysis, aside from the change in aggregation, little morphological/phase/size alteration was found after sonication of the three kinds of ZnO nanoparticles. We then turn our attention to the electronic structure evolution, *i.e.* defect variation in ZnO crystals, which is reflected in the photoluminescence (PL) of ZnO since the PL of ZnO features a UV band gap emission and defect related visible light emission. The PL spectra of the three kinds of ZnO nanoparticles with and without sonication in Fig. 2 show that the three kinds of unsonicated nanoparticles present different PL emissions, and the difference is probably due to the different preparation conditions. For S1 and S2, no obvious PL spectra changes can be observed after sonication with different sonication intensities, as seen from Fig. 2a and b. Fig. 2c shows the PL spectra of S3 with and without sonication treatment, in which the spectra are all composed of a narrow UV emission and a broad visible light emission. Different from S1 and S2, S3 exhibits light emissions that vary with sonication intensities (Fig. 2c). Since there are no dopants incorporated during sonication, the spectra variation in the visible light range is considered to originate from the native defect relaxation.

Why can the defect concentration be adjusted by sonication? A most probable explanation is that when the cavitation bubble collapses, as seen in Scheme 1, the ZnO nanoparticles at the liquid–air interface are moved by bubble collapse to the hot spot with a temperature of 5000 K.[9] Due to the short life time of the hot spot, we assume that the nanoparticle can only be heated locally. Therefore, at the interface of the hot spot and nanoparticle, surface atoms of ZnO nanoparticles are rearranged due to the locally high temperature, followed by a quenching process, leaving a locally annealed nanoparticle. Repeated reactions of nanoparticles with the hot spots then lead to the formation of native defect relaxation and abundant interface defects. As sonication intensity determines the rate of reactions between nanoparticles and the hot spot, it will greatly influence the dynamics of defect relaxation, which would result in different light emissions, as shown in Fig. 2c. It should be highlighted here that the annealing process in the present study is quite different from conventional thermal treatment that is usually used for defect relaxation at high temperature: (i) it can be realized at room temperature, and the extremely high pressure/temperature

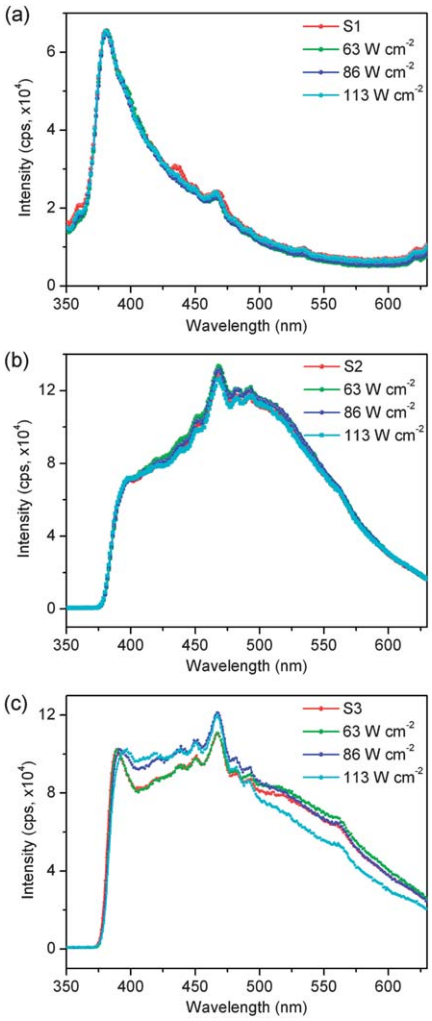

Fig. 2 PL spectra of ZnO particles of different sizes (a) S1, (b) S2, and (c) S3 before and after high intensity ultrasonication with different intensities (63, 86, 113 W cm^{-2}). Excitation wavelength is 325 nm.

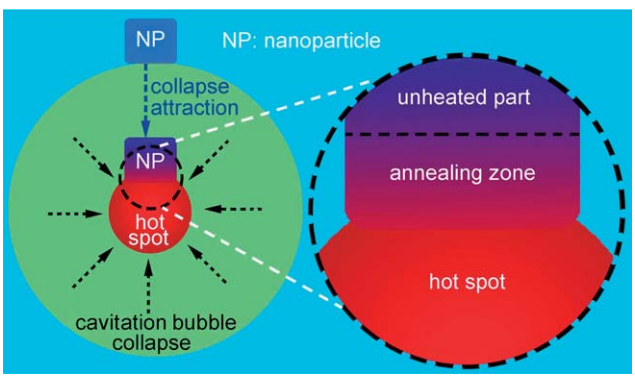

Scheme 1 Snapshot of the localized instantaneous annealing that is involved in high intensity sonication of a bare nanoparticle in liquid. When the nanoparticle is moved by bubble collapse to the hot spot, atom rearrangement is assumed to take place only at the interface of the nanoparticle and hot spot. Due to the short life time of the hot spot, the localized annealing happens instantaneously.

involved in acoustic cavitation is the reason that leads to the native defect relaxation; (ii) it is temporally discontinuous and spatially localized: as seen in Scheme 1, the annealing process takes place only where and when nanoparticles have contact with hot spots, which are actually short lived and micrometer sized.[9] This localized instantaneous annealing could produce ample defect species and active defect relaxation due to extreme non-equilibrium conditions, thus providing a promising way other than thermal treatment for manipulating semiconductor electronic structures.

As for the size-related PL variation, *i.e.* sonication has more effect on S3 than S1 and S2, as demonstrated in Fig. 2, it becomes controversial if one considers that smaller nanoparticles can easily be moved by the collapse to the hot spot and have higher chances to react with the hot spot, thus producing a result in contradiction to Fig. 2. However, a cavitation bubble can only be effective if the bubble is close to the solid nanoparticles, and this is the case if it nucleates on the surface of the nanoparticles. There it grows under ultrasonic irradiation entrapping gas from the liquid medium until the maximum size is reached.[16] It has been reported that the critical particle size, *i.e.* the smallest size to nucleate a cavity, obtained experimentally is hundreds of nanometers,[17] which is much larger than that of S1 and S2, but comparable with that of S3. Therefore, we propose that the size related PL variation shown in Fig. 2 arises from size-dependent cavity nucleation. Modifying surface properties of nanoparticles are expected to decrease the critical crystal size of nuclei, thus enabling a further decrease of the critical size of nanoparticles with detectable native defect relaxation.

As an exploration of the utility of native defect engineering by ultrasonication shown in Fig. 2c, we further performed PEC water splitting measurements for ZnO nanoparticles (S3) with and without sonication, which was done in electrochemical cells containing a ZnO film working electrode made by dip coating of ZnO nanoparticles on fluorine-doped SnO_2 (FTO) glasses, a coiled Pt wire counter-electrode and a $Hg/HgSO_4$ reference electrode, and using K_2SO_4 solution (0.5 M, pH 7) as electrolyte. The measured potentials *vs.* $Hg/HgSO_4$ were converted to the reversible hydrogen electrode (RHE) scale according to the Nernst equation:

$$E_{RHE} = E_{Hg/HgSO_4} + 0.059pH + E^0_{Hg/HgSO_4} \quad (1)$$

where E_{RHE} is the converted potential *vs.* RHE, $E^0_{Hg/HgSO_4}$ is 0.68 V at 25 °C, and $E_{Hg/HgSO_4}$ is the experimentally measured potential against the $Hg/HgSO_4$ reference electrode.

As shown in Fig. 3a, the raw nanoparticles (S3) and S3 treated by sonication with intensity of 113 W cm^{-2} [S3 (113 W cm^{-2})] yield the minimal photocurrent density (0.0025 mA cm^{-2} at 0.45 V *vs.* RHE) in the potential range we studied and at 400 mW cm^{-2} illumination. In contrast, S3 (63 W cm^{-2}) and S3 (86 W cm^{-2}) show pronounced photoactivity: S3 (63 W cm^{-2}) yields a photocurrent density of 0.01 mA cm^{-2}, and S3 (86 W cm^{-2}) achieves a maximum value of 0.02 mA cm^{-2} at 0.45 V *vs.* RHE (Fig. 3a). Furthermore, we have performed amperometric *I–t* studies, at an applied voltage of 0.6 V *vs.* RHE at 100 mW cm^{-2} illumination, to examine the photoresponse of those samples

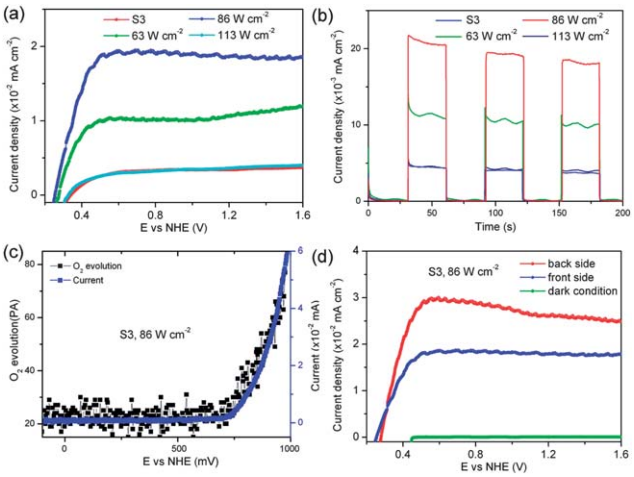

Fig. 3 (a) Photocurrent measurements under tungsten halogen lamp excitation (400 mW cm^{-2}) for S3 before and after sonication with different intensities. (b) Amperometric *I–t* curve of S3 and S3 treated with different sonication intensities at an applied voltage of 0.6 V *vs.* RHE at 400 mW cm^{-2}. (c) Current density (blue curve) and oxygen evolution (dotted) of dip-coated ZnO (S3, 86 W cm^{-2}) film in 0.5 M K_2SO_4 (pH 7). (d) Photocurrent measurements of dip-coated ZnO (S3, 86 W cm^{-2}) film on FTO glass for dark condition (green), front-side illumination (blue) and back-side (red) illumination.

over time and the stability of our constructed PEC devices. As shown in Fig. 3b, all samples show a fast photoresponse, and the steady state photocurrent can be reached within 0.2 s. In addition, the photocurrent densities of all samples shown in Fig. 3b present no obvious decrease indicating the relative stability of our PEC cells.

In order to verify that the anodic current densities observed at potentials higher than 0.3 V are related to oxygen evolution, a home made DEMS (differential electrochemical mass spectrometer) was designed to simultaneously measure released gases during the electrochemical measurement, where the emission of gases was measured by direct contact of the film with a gas-permeable membrane connected to a quadruple mass spectrometer. Taking S3 (86 W cm^{-2}) as the typical example, Fig. 3c shows that the oxygen signals correlate well with the slope of the measured current densities, indicating that the photocurrent production in the present study is related to the photoelectrochemical water splitting, but not the corrosion of ZnO.[18]

Further information can be gathered by illuminating sunlight from front or back side for better elucidating the photocarrier transport properties. Also taking S3 (86 W cm^{-2}) as an example, as shown in Fig. 3d, the photocurrent for back-side illumination is larger than that for front-side illumination. Since the electrons need to travel across the entire thickness of the film (around 500 nm, see Fig. S3†) to the ZnO–FTO interface for collection when illumination is from the front, and the holes need to travel across the entire thickness to the ZnO–H_2O interface for collection when illumination is from the back,[19] the result shown in Fig. 3d indicates the problem of slower electron transport in the film of ZnO nanoparticles. It is thus anticipated that the photocurrent could be further improved by n-doping of the presented ZnO nanoparticles.

Photoelectrochemical results indicate that sonication treatment towards S3 could lead to tunable photoelectrochemical water splitting. Considering the main effects of sonication on ZnO nanoparticles that we have gathered experimentally, the different photoelectrochemical performance could originate from the different light extinction or native defect variation (seen from Fig. 1c and 2c). However, in the present study, the influence of light extinction on enhancing the photocurrent can be eliminated since the maximum photoelectrical enhancement by light scattering was reported to be 10%,[20] which is much lower than in our study (maximum reaching to 800%). Another experimental parameter that could lead to the PEC performance difference is the thickness of the spin coated ZnO film, however, cross-sectional SEM observations (Fig. S3†) reveal that all the ZnO films obtained by spin coating have a roughly 500 nm thickness. Therefore, the different native defect concentrations involved in ZnO nanoparticles are believed to be responsible for the tunable photoelectrochemical behavior.

In order to understand how the native defects vary with sonication, we made a Gaussian fitting to the PL spectrum of S3, and the result is shown in Fig. S4 (ESI†). According to the fitting, the PL spectrum of S3 consists of four emissions: band gap emission, blue emission, green emission and orange emission, which is centered at 392 nm, 428 nm, 488 nm, and 577 nm, respectively. Numerous reports have appeared on native defect species in ZnO nanocrystals, and the defect emission situated at 428 nm (2.90 eV), 488 nm (2.54 eV), and 577 nm (2.15 eV) is most probably related to zinc interstitial defects, oxygen vacancy, and interfacial/oxygen antisite O_{Zn} defects, respectively.[21] According to the calculated defect energy levels, the blue and orange emissions result from shallow energy level defects (SELD), and green emission is related to the deep energy level defect (DELD). Therefore, the manipulation of these native defect concentrations by sonication treatment shown in Fig. 2c can lead to the variation of electronic conductivity of the resulting ZnO nanoparticles, which directly influences the corresponding PEC cell performance.

We thus made a qualitative analysis of the native defect evolution shown in Fig. 2c, and the results are depicted in Table 1. When S3 was subjected to 63 W cm^{-2} sonication, only orange emission that corresponds to SELD shows an intensity increase, thus leading to an increase of the electronic conductivity of ZnO nanoparticles. This well explains the superior PEC performance of S3 (63 W cm^{-2}) compared to that of raw nanoparticles. For S3 (113 W cm^{-2}), the PL spectrum presents increased blue and green emissions, and decreased orange emission, in which both the decrease of orange emission and increase of green emission deteriorate the electronic conductivity. However, the overall PEC performance was not reduced because the deteriorated electronic conductivity is compromised by the increasing concentration of SELD which is related with blue emission. For S3 (86 W cm^{-2}), the PEC cell performance is supposed to be higher than that of S3 (113 W cm^{-2}), since there is no orange emission decrease in the PL spectrum of S3 (86 W cm^{-2}), and this is in good agreement with the PEC result shown in Fig. 3a. With respect to the PEC performance comparison between S3 (63 W cm^{-2}) and S3 (86 W cm^{-2}), the higher performance in the latter case is probably due to the fact that blue emission related defects contribute to the electronic conductivity more than orange emission related defects, even if the increased concentration of green emission related defects reduces the electronic conductivity in S3 (86 W cm^{-2}). Based on the above analysis, the tunable PEC cell performance can be qualitatively explained by the sonication induced evolution of SELD and HELD concentrations, which directly influences the ZnO electronic conductivity.

In summary, we present that an innovative space and time confined annealing involved in high intensity sonication of nanoparticles produces size-specific native defect engineering, which can be adapted for PEC water splitting and yields encouragingly 8-fold increased PEC performance. Different from conventional thermal treatment that is usually used for defect relaxation at high temperature, native defect engineering in the present work is realized at room temperature due to the extreme non-equilibrium conditions involved in acoustic cavitation. The size dependent cavity nucleation at particle surfaces has been proposed to be responsible for the size-related defect relaxation. The tuneable PEC water splitting originates from the electronic conductivity alteration induced by the evolution of SELD/DELD in ZnO nanoparticles treated by sonication. We thus believe that the presented localized instantaneous annealing induced native defect engineering provides a promising alternative for optimizing semiconductor electronic structures for various applications and will advance future studies of reactions between cavitation bubbles and nanoparticles.

Table 1 Native defect intensity evolution from ZnO nanoparticles (sample 3) after high-intensity ultrasonication for 10 min with different intensities, in which '+' stands for concentration increase, '−' stands for concentration decrease, and '0' stands for concentration unchanged

	63 W cm^{-2}	86 W cm^{-2}	113 W cm^{-2}
Zn_I	0	+	+
V_O	0	+	+
O_{Zn}	+	0	−

Acknowledgements

We acknowledge the financial support for this research by "Photocontrol" project of EuFP7 program. H. Wang acknowledges the support of a research fellowship from the Alexander von Humboldt Foundation. L. Jia acknowledges the financial support from National Natural Science Foundation of China (no. 51002158) and the Bundesministerium für Bildung und Forschung BMBF (contract no. 03SF0353A).

Notes and references

1 (*a*) A. Fujishima and K. Honda, *Nature*, 1972, **238**, 37; (*b*) L. Li, S. Chen, X. Wang, Y. Bando and D. Golberg, *Energy Environ. Sci.*, 2012, **5**, 6040; (*c*) G. P. Xu, S. L. Ji, C. H. Miao, G. D. Liu and C. H. Ye, *J. Mater. Chem.*, 2012, **22**, 4890; (*d*) Z. Liu, M. Miyauchi, Y. Uemura, Y. Cui, K. Hara, Z. Zhao, K. Sunahara and A. Furube, *Appl. Phys. Lett.*, 2010, **96**,

233107; (*e*) L. Li, H. Q. Wang, X. S. Fang, T. Y. Zhai, Y. Bando and D. Golberg, *Energy Environ. Sci.*, 2011, **4**, 2586; (*f*) C. H. Miao, S. L. Ji, G. P. Xu, G. D. Liu, L. D. Zhang and C. H. Ye, *ACS Appl. Mater. Interfaces*, 2012, **4**, 4428.

2 (*a*) X. Chen, S. Shen and S. S. Mao, *Chem. Rev.*, 2010, **110**, 6503; (*b*) Z. Zou, J. Ye, K. Sayama and H. Arakawa, *Nature*, 2001, **414**, 625; (*c*) W. X. Zhang and S. H. Yang, *Acc. Chem. Res.*, 2009, **42**, 1617; (*d*) S. D. Tilley, M. Cornuz, K. Sivula and M. Gratzel, *Angew. Chem., Int. Ed.*, 2010, **49**, 6405; (*e*) N. S. Lewis and D. G. Nocera, *Proc. Natl. Acad. Sci. U. S. A.*, 2006, **103**, 15729.

3 (*a*) I. S. Cho, Z. B. Chen, A. J. Forman, D. R. Kim, P. M. Rao, T. F. Jaramillo and X. L. Zheng, *Nano Lett.*, 2011, **11**, 4978; (*b*) Y. Ling, G. Wang, D. A. Wheeler, J. Z. Zhang and Y. Li, *Nano Lett.*, 2011, **11**, 2119; (*c*) X. Feng, K. Shankar, O. K. Varghese, M. T. Paulose, J. LaTempa and C. A. Grimes, *Nano Lett.*, 2008, **8**, 3781; (*d*) K. Shankar, J. I. Basham, N. K. Allam, O. K. Varghese, G. K. Mor, X. Feng, M. Paulose, J. A. Seabold, K. S. Choi and C. A. Grimes, *J. Phys. Chem. C*, 2009, **113**, 6327; (*e*) Y. Qiu, K. Yan, H. Deng and S. Yang, *Nano Lett.*, 2012, **12**, 407; (*f*) X. Fang, L. Wu and L. Hu, *Adv. Mater.*, 2011, **23**, 585.

4 R. van de Krol, in *Electronic Materials: Science & Technology*, ed. R. van de Krol and M. Grätzel, Springer, 2012, vol. 102, ch. 2.

5 (*a*) M. Zhang, W. Luo, Z. Li, T. Yu and Z. Zou, *Appl. Phys. Lett.*, 2010, **97**, 042105; (*b*) N. Iordanova, M. Dupuis and K. M. Rosso, *J. Chem. Phys.*, 2005, **122**, 144305; (*c*) C. Castro, L. Oliveira and M. Guerreiro, *Catal. Lett.*, 2009, **133**, 41.

6 C. S. Enache, D. Lloyd, M. R. Damen, J. Schoonman and R. van de Krol, *J. Phys. Chem. C*, 2009, **113**, 19351.

7 (*a*) Y. Ling, G. Wang, J. Reddy, C. Wang, J. Z. Zhang and Y. Li, *Angew. Chem., Int. Ed.*, 2012, **51**, 4074; (*b*) G. Wang, H. Wang, Y. Ling, Y. Tang, X. Yang, R. C. Fitzmorris, C. Wang, J. Z. Zhang and Y. Li, *Nano Lett.*, 2011, **11**, 3026.

8 (*a*) J. H. Bang and K. S. Suslick, *Adv. Mater.*, 2010, **22**, 1039; (*b*) H. Xu and K. S. Suslick, *J. Am. Chem. Soc.*, 2011, **133**, 9148; (*c*) D. G. Shchukin, E. Skorb, V. Belove and H. Möhwald, *Adv. Mater.*, 2011, **23**, 1922; (*d*) Z. Zheng, X. Zhang, D. Carbo, C. Clark, C.-A. Nathan and Y. Lvov, *Langmuir*, 2010, **26**, 7679; (*e*) U. Shimanovich, V. Volkov, D. Eliaz, A. Aizer, S. Michaeli and A. Gedanken, *Small*, 2011, **8**, 1068; (*f*) A. Gedanken, *Chem.–Eur. J.*, 2008, **14**, 3840.

9 (*a*) K. S. Suslick, *Science*, 1990, **247**, 1439; (*b*) K. S. Suslick, *MRS Bull.*, 1995, **20**, 29.

10 (*a*) V. Belova, D. A. Gorin, D. G. Shchukin and H. Möhwald, *Angew. Chem., Int. Ed.*, 2010, **49**, 7129; (*b*) E. V. Skorb, D. G. Shchukin, H. Möhwald and D. V. Andreeva, *Nanoscale*, 2010, **2**, 722.

11 S. J. Doktycz and K. S. Suslick, *Science*, 1990, **247**, 1067.

12 D. G. Shchukin, D. A. Gorin and H. Möhwald, *Langmuir*, 2006, **22**, 7400.

13 (*a*) D. V. Radziuk, W. Zhang, D. Shchukin and H. Möhwald, *Small*, 2010, **6**, 545; (*b*) D. Radziuk, D. Grigoriev, W. Zhang, D. Su, H. Möhwald and D. Shchukin, *J. Phys. Chem. C*, 2010, **114**, 1835.

14 H. M. Xiong, D. G. Shchukin, H. Möhwald, Y. Xu and Y.-Y. Xia, *Angew. Chem., Int. Ed.*, 2009, **48**, 2727.

15 (*a*) R. Viswanatha, S. Sapra, B. Satpati, P. V. Satyam, B. N. Dev and D. D. Sarma, *J. Mater. Chem.*, 2004, **14**, 661; (*b*) H. Wang, N. Koshizaki, L. Li, L. Jia, K. Kawaguchi, X. Li, A. Pyatenko, Z. Swiatkowska-Warkocka, Y. Bando and D. Golberg, *Adv. Mater.*, 2011, **23**, 1865.

16 V. Belova, D. G. Shchukin, D. A. Gorin, A. Kopyshev and H. Möhwald, *Phys. Chem. Chem. Phys.*, 2011, **13**, 8015.

17 H. Iwasaki, H. Hosokawa, M. Mabuchi and K. Higashi, *Mater. Sci. Technol.*, 2000, **16**, 1295.

18 A. Ramírez, P. Bogdanoff, D. Friedrich and S. Fiechter, *Nano Energy*, 2012, **1**, 282.

19 Y. Liang, T. Tsubota, L. P. A. Mooij and R. van de Krol, *J. Phys. Chem. C*, 2011, **115**, 17594.

20 H. Wang, M. Miyauchi, Y. Ishikawa, A. Pyatenko, N. Koshizaki, Y. Li, L. Li, X. Li, Y. Bando and D. Golberg, *J. Am. Chem. Soc.*, 2011, **133**, 19102.

21 (*a*) B. Q. Cao, W. P. Cai and H. B. Zeng, *Appl. Phys. Lett.*, 2006, **88**, 161101; (*b*) H. B. Zeng, W. P. Cai, J. L. Hu, G. T. Duan, P. S. Liu and Y. Li, *Appl. Phys. Lett.*, 2006, **88**, 171910; (*c*) H. Q. Wang, G. Z. Wang, L. C. Jia, C. J. Tang and G. H. Li, *J. Phys. D: Appl. Phys.*, 2007, **40**, 6549; (*d*) H. B. Zeng, G. T. Duan, Y. Li, S. K. Yang, X. X. Xu and W. P. Cai, *Adv. Funct. Mater.*, 2010, **20**, 561.

